J Mater Sci (2008) 43:6784–6797
DOI 10.1007/s10853-008-2934-1

# Dielectric and piezoelectric properties of $(1 - x)(Na_{0.5}K_{0.5})NbO_3$–$xBaTiO_3$ ceramics

**Cheol-Woo Ahn · Chang-Hak Choi · Hwi-Yeol Park · Sahn Nahm · Shashank Priya**

Received: 25 April 2008 / Accepted: 5 August 2008 / Published online: 2 October 2008


**Abstract** This manuscript reviews the studies on phase transitions, synthesis, and piezoelectric/dielectric properties of $(1 - x)(Na_{0.5}K_{0.5})NbO_3$–$xBaTiO_3$ ceramics ($0.0 \leq x \leq 1.0$). Three phase transition regions were observed in $(1 - x)(Na_{0.5}K_{0.5})NbO_3$–$xBaTiO_3$ ceramics corresponding to orthorhombic, tetragonal, and cubic phases. The composition $0.95(Na_{0.5}K_{0.5})NbO_3$–$0.05BaTiO_3$, which lies on the boundary of orthorhombic and tetragonal phases, was found to exhibit excellent piezoelectric properties. The properties of this composition were further improved by addition of various additives making it suitable for multilayer actuator application. The composition $0.06(Na_{0.5}K_{0.5})NbO_3$–$0.94BaTiO_3$ was found to lie on the boundary of tetragonal and cubic phases. This composition exhibited the microstructure with small grain size and excellent dielectric properties suitable for multilayer ceramic capacitor application. Based on the studies reported in literature, we expect the modified $(1 - x)(Na_{0.5}K_{0.5})NbO_3$–$xBaTiO_3$ system to become the leading lead-free candidate for piezoelectric and dielectric components.

C.-W. Ahn · S. Priya
Department of Materials Science and Engineering, Virginia Polytechnic Institute and State University, Blacksburg, VA 24061, USA
e-mail: spriya@vt.edu

S. Priya
e-mail: spriya@vt.edu

C.-H. Choi · H.-Y. Park · S. Nahm (✉)
Department of Materials Science and Engineering, Korea University, 1–5 Ka, Anam-Dong, Sungbuk-Ku, Seoul 136–713, South Korea
e-mail: snahm@korea.ac.kr

## Introduction

$Pb(Zr,Ti)O_3$ (PZT)-based ceramics have excellent dielectric and piezoelectric properties and are currently the dominant materials for actuators, sensors, and resonators [1]. However, the Pb element in these materials presents an environmental problem. Thus, the research is now focused on finding an alternative for PZTs. In the past two decades, a lot of publications and patents have been reported on lead-free piezoelectrics [2–47]. Out of all the possible choices (see Table 1), $(Na,K)NbO_3$ (NKN)-based ceramics (e.g., solid solution of NKN–$LiNbO_3$, NKN–$LiTaO_3$, NKN–$LiSbO_3$, NKN–$Li(Nb, Ta, Sb)O_3$, NKN–$BaTiO_3$, NKN–$SrTiO_3$, and NKN–$CaTiO_3$) have received considerable attention mainly for two reasons (i) piezoelectric properties exist over a wide range of temperature and (ii) several possibilities for substitution and additions [2, 39–47].

Recently, we have reported the dielectric and piezoelectric properties of $0.95(Na_{0.5}K_{0.5})NbO_3$–$0.05BaTiO_3$ (0.95NKN–0.05BT) ceramics. The piezoelectric coefficients of this composition were measured on a disk-shaped sample and were found to be $k_p = 0.36$, $d_{33} = 225$ pC/N, and $\varepsilon_{33}{}^T/\varepsilon_0 = 1058$ [40, 41]. For polycrystalline lead-free ceramics, this magnitude is quite high (see Table 1 for comparison) and opens the possibility for realizing lead-free multilayer actuators. NKN–BT system has also been studied to find a suitable multilayer ceramic capacitor (MLCC) composition. The composition given by the formulation 0.06KNN–0.94BT was found to have excellent dielectric properties [48]. Hence, $(1 - x)$KNN–$x$BT system comprises compositions that exhibit excellent dielectric and piezoelectric properties. In this review paper, we summarize the synthesis, structure, phase transitions, microstructure, and piezoelectric properties of $(1 - x)(Na_{0.5}K_{0.5})NbO_3$–$xBaTiO_3$ (NKN–BT) ceramics. The effect of several

**Table 1** Dielectric and piezoelectric properties of the prominent lead-free systems

| System | $d_{33}$ (pC/N) | $\varepsilon_3^T/\varepsilon_o$ | tan $\delta$ | $k_p$ | $T_d/T_c$ (°C) |
|---|---|---|---|---|---|
| NBT–KBT–BT [2, 24] | 183 | 770 | 0.03 | 0.37 | 100/290 |
| NBT–KBT–LBT [2, 19] | 216 | 1,550 | 0.03 | 0.40 | 160/350 |
| NKN–$LiNbO_3$ [2, 9] | 235 | 500 | 0.04 | 0.42 | –/460 |
| NKN–$LiTaO_3$ [8] | 268 | 570 | 0.01 | 0.46 | –/430 |
| NKN–$LiSbO_3$ [2, 10] | 283 | 1,288 | 0.02 | 0.50 | –/392 |
| NKN–Li(Nb, Ta, Sb)$O_3$ [39] | 308 | 1,009 | 0.02 | 0.51 | –/339 |
| NKN–$BaTiO_3$ [40, 41] | 225 | 1,058 | 0.03 | 0.36 | –/304 |
| NKN–$SrTiO_3$ [42] | 220 | 1,447 | 0.02 | 0.40 | – |
| NKN–$CaTiO_3$ [43] | 241 | 1,316 | 0.09 | 0.40 | –/306 |

$T_d$: depolarization temperature; $T_c$: Curie temperature

additives on the microstructure and piezoelectric properties is also reviewed.

## Synthesis, structural analysis, phase transitions, and ferroelectricity [2, 4, 7–10, 39–41, 43–45, 48–50]

Pure NKN and solid solution $(1-x)$NKN–$x$BT modified with various additives (CuO, $MnO_2$, $WO_3$, and ZnO) were synthesized from oxides of >99% purity using conventional solid-state synthesis. The oxide powders of $Na_2CO_3$, $K_2CO_3$, $Nb_2O_5$, $BaCO_3$, and $TiO_2$ (all obtained from High Purity Chemicals, Saitama, Japan) were mixed for 24 h in a nylon jar with zirconia balls. The mixed powders were dried and then calcined at 950–1000 °C for 3 h in air. Calcined powders were milled with additives (all obtained from High Purity Chemicals, Saitama, Japan) for 48 h and dried. The dried powders were pressed into disks under a pressure of 100 kgf/cm$^2$ and the specimens were sintered in the temperature range 925–1350 °C for 2–10 h in air. The ball milling time before and after the calcination, calcination temperature, sintering temperature, and sintering time are listed in Table 2 for pure and modified NKN and NKN–BT system.

The crystal structure and the microstructure of the specimens were examined by X-ray diffractometer (XRD, Rigaku D/max-RC, Japan), scanning electron microscope (SEM, Hitachi S-4300, Japan), and transmission electron microscope (TEM: Hitachi H-9000NAR, Japan). Chemical analysis was conducted using energy dispersive spectroscopy (EDS, Horiba EX-200, Japan). The samples were poled in silicone oil at 120 °C by applying a DC field of 3 to 4 kV/mm for 60 min (see Table 2 for poling temperature and field). All electrical measurements were done on aged samples (24 h after poling). The electromechanical, piezoelectric, and dielectric properties were determined using a $d_{33}$ meter (Micro-Epsilon Channel Product DT-3300, Raleigh, NC) and an impedance analyzer (Agilent Technologies, Model HP 4194, Santa Clara, CA). The dielectric constant as a function of temperature was obtained using an LCR meter (HP model 4284). The polarization electric-field behavior was determined using a home-built modified Sawyer-Tower circuit.

Figure 1 shows the X-ray diffraction patterns of specimens in $(1-x)$NKN–$x$BT ceramics. As seen in Fig. 1a and b, the crystal structure changed from orthorhombic to tetragonal phase in the range $0.0 \leq x \leq 0.1$, and from tetragonal to cubic phase around $x = 0.2$. The system exhibited cubic phase in the range of $0.2 < x < 0.9$ and the phase was changed to tetragonal when $x$ exceeded 0.94, as shown in Fig. 1a and c. Thus, three phase transition regions were identified in $(1-x)$NKN–$x$BT ceramics. The inset in Fig. 1b shows the secondary phases of $K_6Nb_{10.8}O_{30}$ (at NKN), $KTiNbO_5$, and $Ba_6Ti_2Nb_8O_{30}$ (at 0.95NKN–0.05BT)

**Table 2** Experimental conditions of the pure the and the modified $(Na_{0.5}K_{0.5})NbO_3$ and $(1-x)(Na_{0.5}K_{0.5})NbO_3$–$x$$BaTiO_3$ systems

| System | Cal. (°C/h) | Sin. (°C/h) | Poling (kV/mm, °C, min) |
|---|---|---|---|
| NKN | 950/3 | 1,090/2 | 4, 120, 60 |
| NKN + ZnO | 950/3 | 1,050/2 | 4, 120, 60 |
| NKN + $MnO_2$ | 950/3 | 1,050/2 | 4, 120, 60 |
| NKN + $WO_3$ | 950/3 | 1,090/2 | 4, 120, 60 |
| NKN + CuO | 950/3 | 950/2 | 4, 120, 60 |
| NKN + CuO + ZnO | 950/3 | 925/2 | 4, 120, 60 |
| 0.99NKN–0.01BT ~ 0.93NKN–0.07BT | 950/3 | 1,000–1,150/2 | 3–4, 120, 60 |
| 0.9NKN–0.1BT ~ BT | 1,000/3 | 1,100–1,350/2–7 | 4, 120, 60 |
| 0.95NKN–0.05BT + $MnO_2$ | 950/3 | 1,050/2 | 4, 120, 60 |
| 0.95NKN–0.05BT + ZnO | 950/3 | 1,040/2–10 | 4, 120, 60 |
| 0.95NKN–0.05BT + CuO | 950/3 | 950/2–10 | 4, 120, 60 |
| 0.95NKN–0.05BT + CuO + $MnO_2$ | 950/3 | 950/2–10 | 4, 120, 60 |

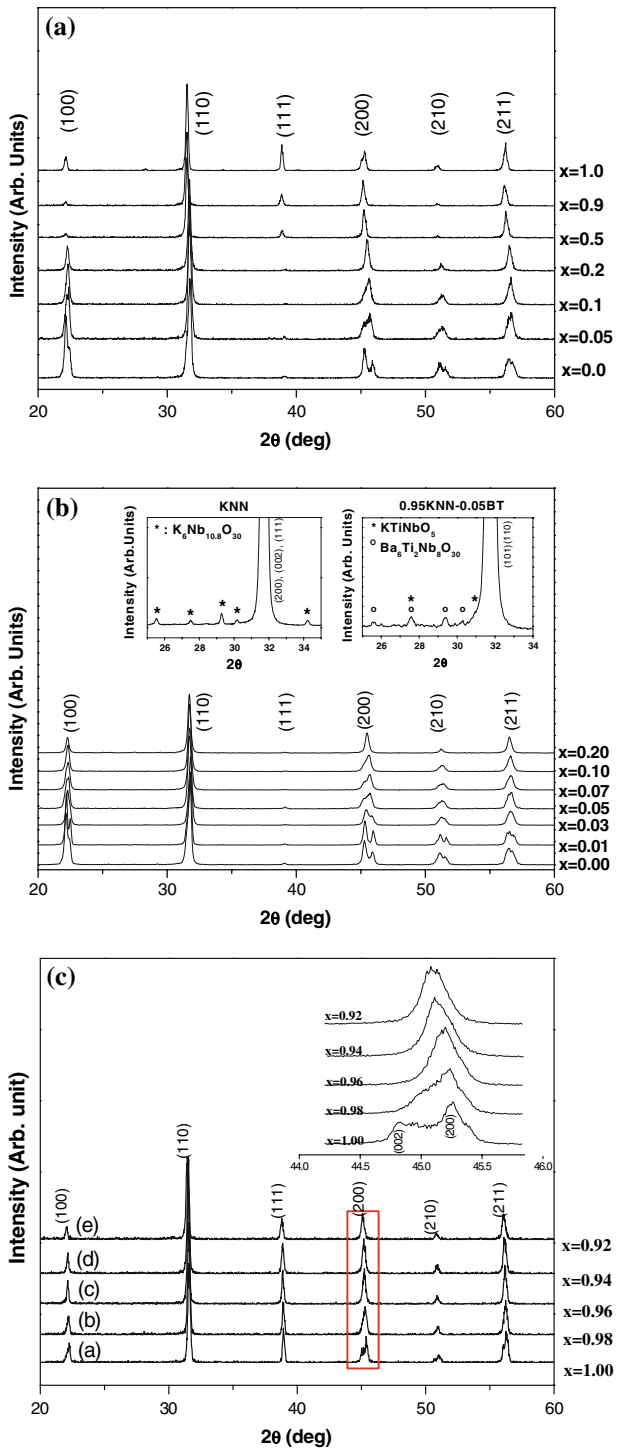


**Fig. 1** X-ray diffraction patterns of $(1 - x)(Na_{0.5}K_{0.5})NbO_3$–$xBaTiO_3$ ceramics: (**a**) $0.0 \leq x \leq 1.0$, (**b**) $0.00 \leq x \leq 0.20$, and (**c**) $0.92 \leq x \leq 1.00$

commonly observed in the specimens sintered at temperatures higher than 1000 °C. These phases are related to the volatilization of $Na_2O$ at higher sintering temperatures. More information on $Na_2O$ volatilization is provided in microstructure section of this paper.

Figure 1b shows the X-ray diffraction patterns of $(1 - x)$ NKN–$x$BT ceramics in the range $0.0 \leq x \leq 0.2$ which illustrates the phase transition from orthorhombic to tetragonal phase. All the peaks were indexed in terms of cubic perovskite unit cell. Rietveld refinement was done to investigate the detailed crystal structure in the range $0.2 \leq x \leq 0.7$, as shown in Table 3. The specimens with $x \leq 0.02$ had an orthorhombic structure with Bmm2 space group. A tetragonal structure with P4 mm space group was found to exist for $x = 0.03$ and the fraction of the tetragonal phase was found to increase with the mole fraction of BT. The specimen with $x = 0.07$ showed a tetragonal structure. Thus, the region in which both orthorhombic and tetragonal phases coexist corresponds to the compositions given by $0.03 \leq x \leq 0.06$. The samples with BT ratio higher than 0.1 had a cubic structure with Pm3 m space group symmetry. These trends of phase transition are very similar to that of $(1 - x)NaNbO_3$–$xBaTiO_3$ (NN–BT) as shown in Fig. 2a and have been reported in literature as illustrated in Fig. 2c [45, 49].

Figure 1c shows the XRD patterns of $(1 - x)$NKN–$x$BT ceramics in the range $0.92 \leq x \leq 1.00$ sintered at 1300 °C for 2 h. All the peaks were indexed in terms of cubic perovskite unit cell. The inset of Fig. 1c exhibits the variation of (200) and (002) peaks of BT ceramics near $2\theta = 45°$ which merged into a single (200) peak with decreasing $x$ value. This result indicated that when the ratio of BT was higher than 0.98 in $(1 - x)$NKN–$x$BT ceramics, it exhibits a tetragonal structure. The crystal structure changed from tetragonal to cubic when the BT ratio was lower than 0.98. Thus, the region for coexistence of the tetragonal and cubic phase corresponds to the composition $0.92 < x < 0.96$. Although the phase transition of the NKN-rich region showed similar tendency to NN–BT ceramics, BT-rich compositions of $(1 - x)$NKN–$x$BT ceramics had a trend similar to the phase transition in $(1 - x)KNbO_3$–$xBaTiO_3$ (KN–BT) system, as shown in Fig. 2b [50].

The phase transitions were verified by monitoring the change in $T_{O-T}$ (orthorhombic to tetragonal structure) and $T_c$ (Curie temperature) as a parameter of composition, as shown in Fig. 3. The $T_c$ of pure NKN specimen was found to be ~420 °C, and it decreased with the increase of BT ratio in $(1 - x)$NKN–$x$BT ceramics, as shown in Fig. 3a. A Curie temperature of 0.95NKN–0.05BT ceramics was found to be 320 °C. The transition temperature, $T_{O-T}$, was observed at ~200 °C for pure NKN ceramics, which decreased toward near room temperature in 0.95NKN–0.05BT ceramics, as shown in Fig. 3a and c. These results are in agreement with that observed by XRD analysis. As expected, Pb-free ceramics showed much higher piezoelectric constant at the compositions in which $T_{O-T}$ was located near room temperature, as shown in Fig. 3c [2, 4, 7–10, 39–41, 43]. The temperature dependence of the

**Table 3** Crystal structure of $(1 - x)(Na_{0.5}K_{0.5})NbO_3$–$xBaTiO_3$ ceramics [44]

| $x$ | 0.02 | 0.03 | 0.04 | 0.05 | 0.06 | 0.07 |
|---|---|---|---|---|---|---|
| Space group | Bmm2 | Bmm2/P4 mm | Bmm2/P4 mm | Bmm2/P4 mm | Bmm2/P4 mm | Bmm2/P4 mm |
| Cell parameter (Bmm2, Å) | a = 5.6898(5) | a = 5.6594(3) | a = 5.6537(5) | a = 5.6520(6) | a = 5.6545(5) | a = 5.6471(7) |
| | b = 3.9518(5) | b = 3.9541(2) | b = 3.9602(3) | b = 3.9598(4) | b = 3.9656(4) | b = 3.9638(5) |
| | c = 5.6418(5) | c = 5.6356(3) | c = 5.6360(5) | c = 5.6365(6) | c = 5.6321(5) | c = 5.6875(7) |
| Cell Parameter | – | a = 3.9674(3) | a = 3.9663(4) | a = 3.9692(2) | a = 3.9661(2) | a = 3.9708(1) |
| (P4 mm, Å) | | c = 4.0146(6) | c = 4.0126(6) | c = 4.0102(4) | c = 4.0131(2) | c = 4.0028(1) |
| Weight ratio of orthorhombic to tetragonal | 100% | 58.20% | 32.60% | 28.40% | 23.80% | 3.90% |
| | 0% | 41.80% | 67.40% | 71.60% | 76.20% | 96.10% |

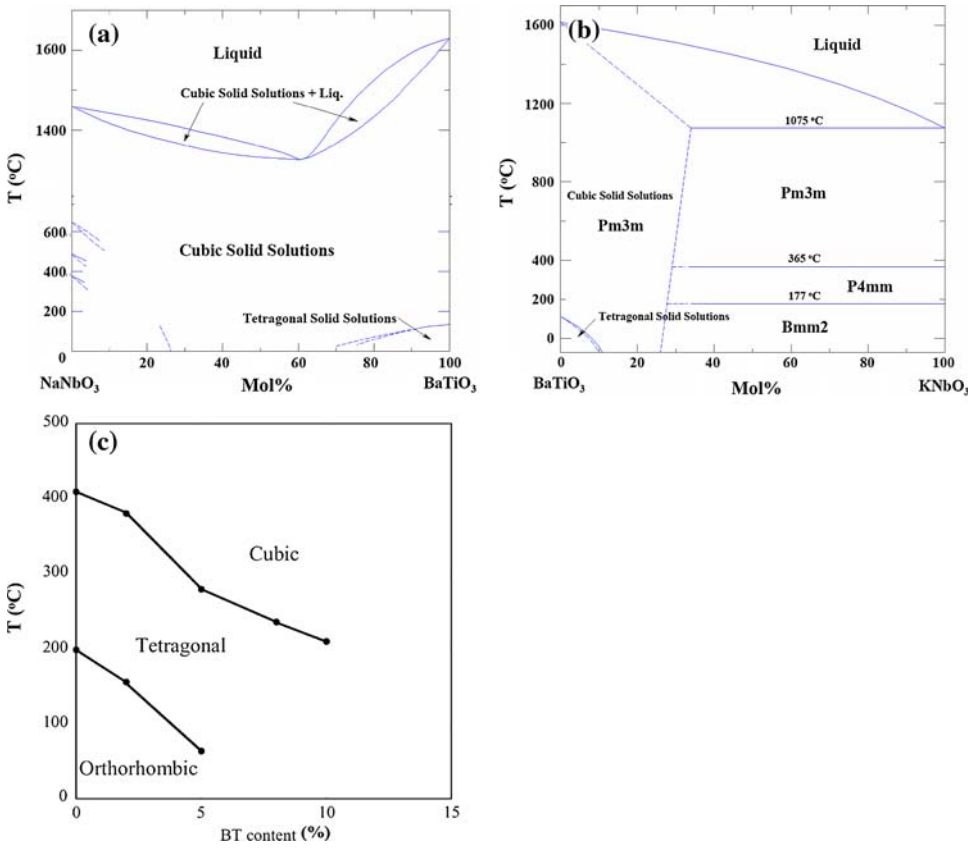


**Fig. 2** Phase diagram of alkali niobate—barium titanate system: (**a**) $(1 - x)NaNbO_3$–$xBaTiO_3$, (**b**) $(1 - x)KNbO_3$–$xBaTiO_3$, and (**c**) $(1 - x)(Na_{0.5}K_{0.5})NbO_3$–$xBaTiO_3$ [45, 49, 50]

dielectric constant and the loss tangent for the $(1 - x)$ NKN–$x$BT ceramics with $0.92 \leq x \leq 1.00$ is shown in Fig. 3b. The Curie temperature increased with BT content and for 0.06NKN–0.94BT ceramics it was found to be around room temperature. For the specimen of composition 0.08NKN–0.92BT, the $T_c$ was less than room temperature. These trends were similar to those observed from XRD patterns, as shown in Fig. 1c.

The dielectric and XRD results were also consistent with that predicted from polarization (P)—electric field (E) behavior. Figure 4 shows the variation of P–E curves for $(1 - x)$NKN–$x$BT ceramics with BT content. The composition corresponding to 0.95NKN–0.05BT showed higher remanent polarization ($P_r$) and strain than those of pure NKN ceramics. The compositions corresponding to 0.5NKN–0.5BT did not show any ferroelectricity illustrating the cubic phase as seen in Fig. 1. The composition 0.05NKN–0.95BT had much lower coercive field ($E_c$) and $P_r$ than those of 0.95NKN–0.05BT and pure NKN ceramics, indicating that ferroelectric properties are higher in the mixed orthorhombic and tetragonal regions.

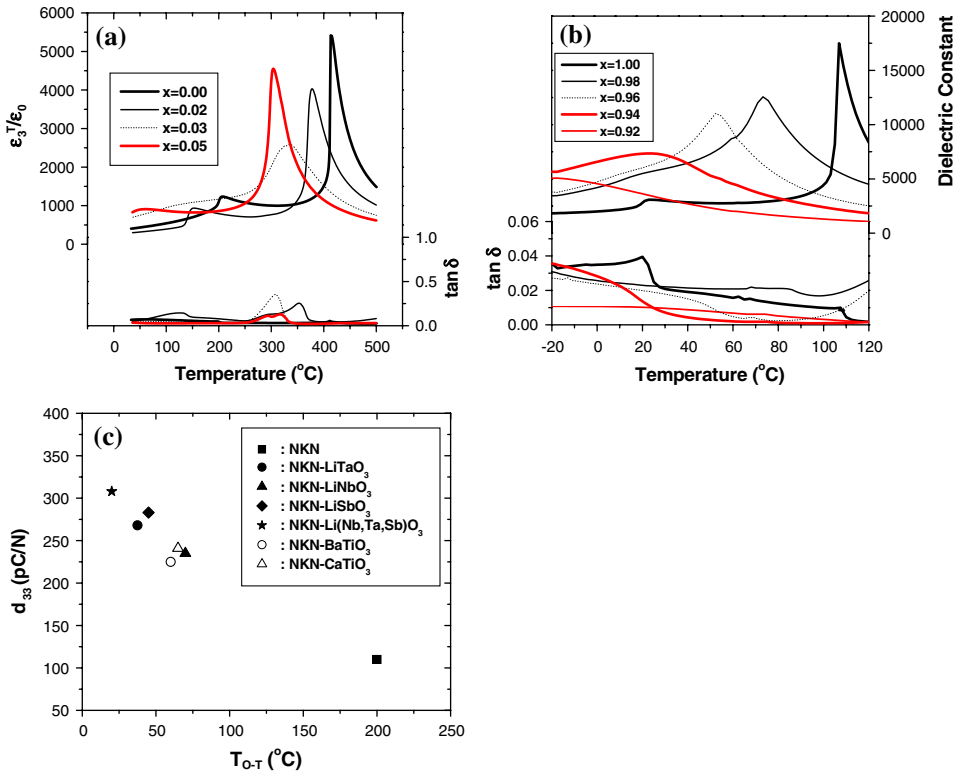


**Fig. 3** Variation of dielectric constant and loss factor as a function of temperature for $(1 - x)(Na_{0.5}K_{0.5})NbO_3$–$xBaTiO_3$ ceramics and piezoelectric constants of NKN-based ceramics with various $T_{O-T}$ ($T_{O-T}$: phase transition temperature from orthorhombic to tetragonal structure): (**a**) $0.00 \leq x \leq 0.05$, (**b**) $0.92 \leq x \leq 1.00$, and (**c**) piezoelectric constants of NKN-based ceramics with various $T_{O-T}$ [2, 4, 7–10, 39–41, 43

## Microstructure and poling of NKN–BT ceramics: $Na_2O$ volatilization [40, 41]

The microstructures of NKN–BT ceramics are shown in Figs. 5–7. As shown in Fig. 5, pure NKN and 0.95NKN–0.05BT ceramics showed larger grain size than 0.05NKN–0.95BT and BT ceramics. The compositions corresponding to 0.9NKN–0.1BT and 0.8NKN–0.2BT showed small grain size of the order of 0.2 μm compared with pure NKN and 0.95NKN–0.05BT ceramics, as shown in Fig. 6. The microstructure showed round and small grains in the composition range $0.92 \leq x \leq 1.00$ compared with the rectangular and large grains in the composition range $0.00 \leq x \leq 0.06$, as shown in Figs. 6 and 7. The grain size decreased with decreasing BT ratio content from 1.2 μm to 0.2 μm. In applications such as MLCCs, the grain size of the specimen should be less than 0.5 μm which makes 0.94BT–0.06NKN ceramics with grain size of 0.4 μm, dielectric constant of 7,500, and tan $\delta$ of less than 1.0% very promising.

In piezoelectric applications, the specimens must have high resistivity in order to pole them easily. Thus, complex impedances of the 0.95NKN–0.05BT specimens sintered at 1060 °C were measured at 120 °C in air, as shown in Fig. 8. The resistance of the specimen was found to be very low of the order of 3070 MΩ cm compared with $10^4$–$10^7$ MΩ cm for PZT-based ceramics [51]. The low resistivity might be explained by $Na_2O$ volatilization, which was expected to cause the formation of second phases (as shown in XRD patterns in Fig. 1b). In order to reduce the $Na_2O$ volatilization in 0.95NKN–0.05BT ceramics sintered at 1060 °C, the specimens were sintered under muffled condition. The resistivity of the specimen sintered under muffled condition was found to be $17.9 \times 10^3$ MΩ cm, which was much higher than that of the specimen sintered in air atmosphere.

The effect of $Na_2O$ volatilization on the microstructure of 0.95NKN–0.05BT ceramics was investigated using SEM, EDS, and TEM analyses. Figure 9 shows the SEM and TEM images of the specimens sintered at various temperatures. Liquid phase formation was observed in all the specimens sintered at temperatures higher than 1050 °C. It can be expected that liquid phase assists the densification of the specimens during the sintering and promotes the grain growth. EDS analysis was conducted on the specimen sintered at 1125 °C to identify the composition of the liquid phase. Figures 10a and b illustrates the EDS spectra taken from the matrix and liquid phase, respectively, and the results of composition analysis are summarized in Table 4. In the matrix, Na, K, Nb, Ba, and Ti ions were found and the composition of the matrix was the same as the starting composition of 0.95NKN–0.05BT. In the liquid phase, high concentration of K and Nb ions was detected with only small concentration of Na ions. Ba and Ti ions were also found in the liquid phase. Therefore, the liquid phase was considered to be Na deficient and was

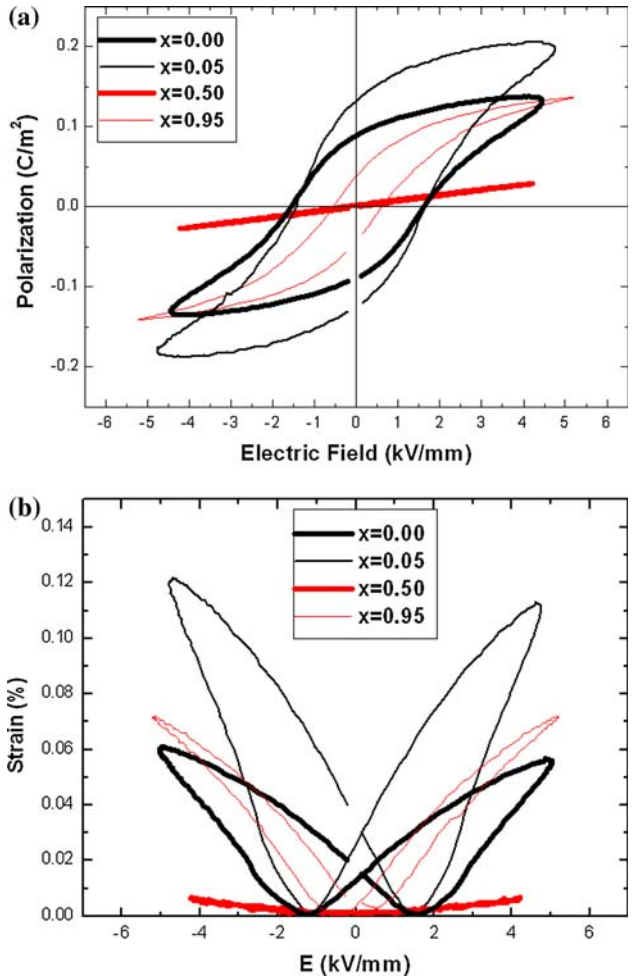


**Fig. 4** Polarization vs. electric field curves of $(1-x)(Na_{0.5}K_{0.5})NbO_3$–$xBaTiO_3$ ceramics

probably produced by the $Na_2O$ volatilization. It was analyzed that 0.95NKN–0.05BT phase decomposes into the liquid and second phases during the sintering at high temperatures. Using the results of the EDS analysis and XRD patterns, the formation of the liquid phase and secondary phases ($KTiNbO_5$ and $Ba_6Ti_2Nb_8O_{30}$) can be explained through the following reaction:

$$0.95(Na_{0.5}K_{0.5})NbO_3 - 0.05BaTiO_3 \rightarrow 0.95(Na_{0.12}K_{0.49})Nb_{0.98}O_{2.76} - 0.05Ba_{0.84}Ti_{0.84}O_{2.52} + 0.0062KTiNbO_5 + 0.0015Ba_6Ti_2Nb_8O_{30} + 0.18Na_2O\uparrow$$

The above expression shows how $Na_2O$ volatilization during sintering leads to decomposition of the 0.95NKN–0.05BT phase into secondary phases ($KTiNbO_5$ and $Ba_6Ti_2Nb_8O_{30}$) and the liquid phase, with a resulting composition close to $0.95(Na_{0.12}K_{0.49})Nb_{0.98}O_{2.76}$–$0.05Ba_{0.84}Ti_{0.84}O_{2.52}$. The calculated composition of the liquid phase is shown in Table 5, which was similar to that obtained from the EDS analysis.

## Piezoelectric properties and additive effect: modified NKN and NKN–BT ceramics for actuator, resonator and sensor applications

### NKN + additives ceramics [46, 52]

Figure 11 shows the piezoelectric properties of $(Na_{1-x}K_x)NbO_3$ ceramics. It was found that the piezoelectric properties of $(Na_{0.5}K_{0.5})NbO_3$ (NKN) was better than the other compositions with coefficients given as $k_p = 0.39$ and $d_{33} = 115$ pC/N. This result is in agreement with that reported in literature by several researchers and is associated with the coexistence of the orthorhombic phases [46]. Various additives were experimented in the NKN system which can be classified in three categories (i) sintering agent (CuO, ZnO, $MnO_2$), (ii) softener ($WO_3$), and (iii) hardener (CuO, $MnO_2$). The effects of different additives on the dielectric and piezoelectric properties are shown in Table 6. The additive effects of ZnO and CuO are discussed here in detail as these ceramics showed high $d_{33}$ and $Q_m$ values.

Figure 12a and b shows the XRD patterns and SEM image of the ZnO-added NKN specimens. Pure NKN specimens showed a porous microstructure compared with ZnO-added NKN specimen (as seen in Figs. 5 and 6). A large volume fraction of liquid phase was found in the microstructure for NKN + 1.5 mol% ZnO specimen, as shown in the inset of Fig. 12b). The density of ZnO-added NKN specimen was ~94% which was slightly higher than that of pure NKN specimen (~92%). Thus, this higher density might be correlated to the formation of the liquid phase which promotes grain growth. The variation of $T_c$ in ZnO-added NKN ceramics is shown in Fig. 13. This change in $T_c$ may be related to the Zn substitution on Nb-site in NKN ceramics. Thus, Zn addition results not only in better density assisted by liquid phase but also in improvement of piezoelectric properties by incorporating into perovskite lattice.

Figure 14 shows the XRD patterns and SEM image of the NKN + $x$ mol% CuO specimens. The microstructure of NKN + 1.5 mol% CuO specimens sintered at 950 °C was similar to that of pure NKN ceramics, as shown in Figs. 5a and 14b. A large volume fraction of liquid phase was also found in the microstructure of the specimens sintered at 1050 °C for 2 h, as shown in the inset of Fig. 14b. Thus, the high density of 91% in the CuO-added NKN ceramics sintered at 950 °C might be explained by liquid phase sintering. The $T_c$ of the CuO-added NKN ceramics decreased slightly from 420 °C to 400 °C, as shown in Fig. 15. This change in $T_c$ was correlated with the Cu substitution on Nb-site, since $d_{33}$ and dielectric constant were decreased and the $Q_m$ value was increased, as shown

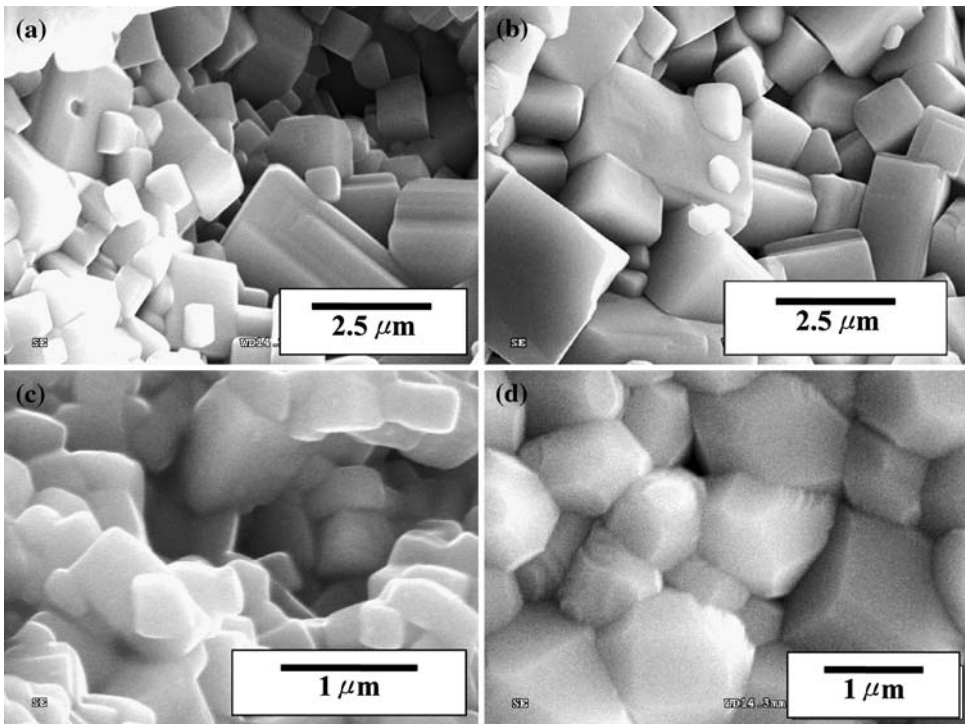


**Fig. 5** SEM images of $(1 - x)(Na_{0.5}K_{0.5})NbO_3$–$xBaTiO_3$ ceramics: (**a**) $x = 0.00$, (**b**) $x = 0.05$, (**c**) $x = 0.95$, and (**d**) $x = 1.00$

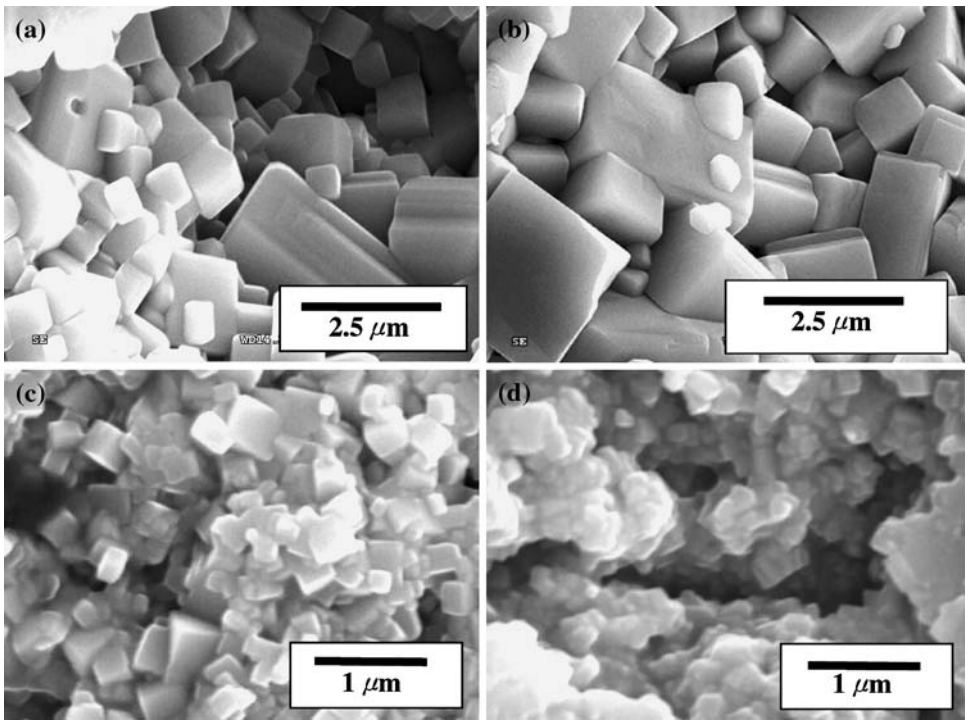


**Fig. 6** SEM images of $(1 - x)(Na_{0.5}K_{0.5})NbO_3$–$xBaTiO_3$ ceramics: (**a**) $x = 0.00$, (**b**) $x = 0.05$, (**c**) $x = 0.10$, and (**d**) $x = 0.20$

in Table 6. Therefore, CuO is a good hardener as well as sintering agent in NKN ceramics.

NKN–BT + additives ceramics [47, 53, 54]

Figure 16 summarizes the dielectric and piezoelectric properties of $(1 - x)$NKN–$x$BT ceramics. Excellent piezoelectric property of $d_{33} = 225$ pC/N and dielectric constant of 1058 was found for the composition 0.95NKN–0.05BT, which lies on the boundary of orthorhombic and tetragonal phases. Muffling condition was required to obtain high poling efficiency in 0.95NKN–0.05BT ceramics when they were sintered at temperatures higher than 1000 °C, as seen in Fig. 8. However, the

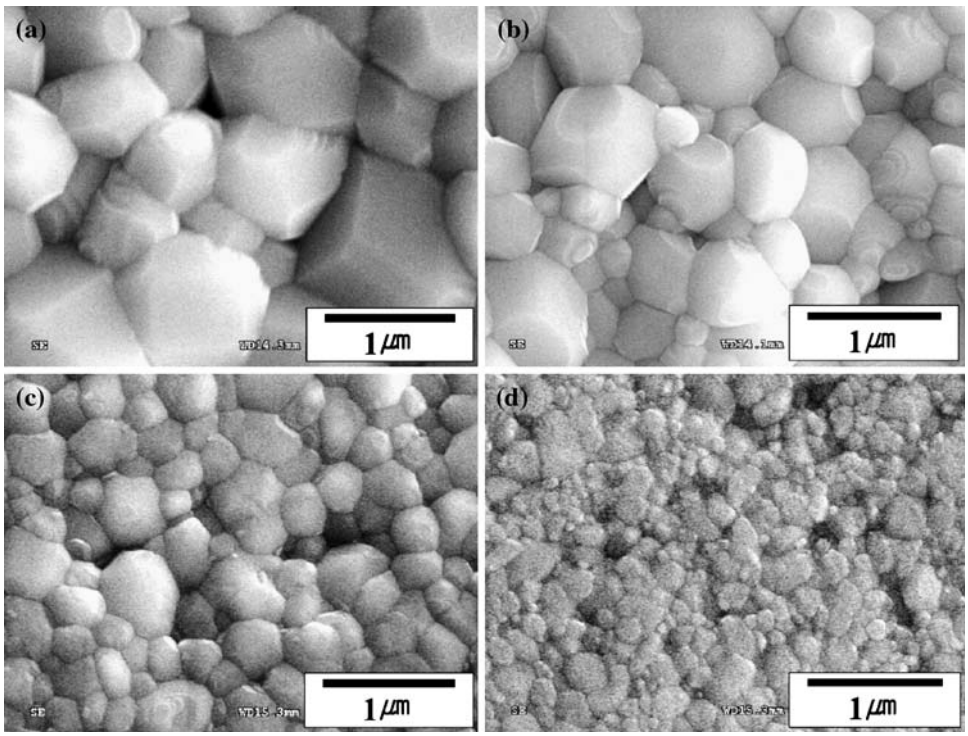


**Fig. 7** SEM images of $(1 - x)(Na_{0.5}K_{0.5})NbO_3$–$xBaTiO_3$ ceramics: (**a**) $x = 1.00$, (**b**) $x = 0.97$, (**c**) $x = 0.94$, and (**d**) $x = 0.92$

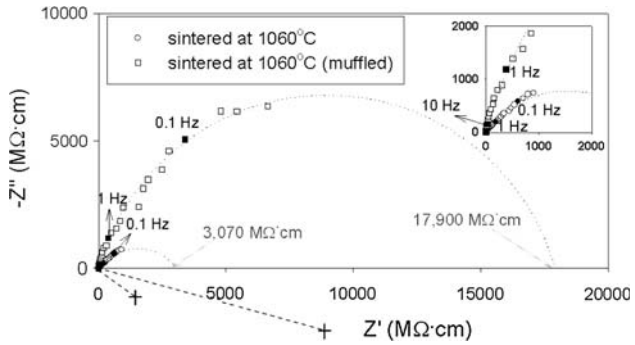


**Fig. 8** Complex impedance spectra of $0.95(Na_{0.5}K_{0.5})NbO_3$–$0.05BaTiO_3$ ceramics sintered at 1060 °C with and without muffling (at 120 °C)

control of muffling condition was not easy. Thus, several additives were added to 0.95NKN–0.05BT ceramics in order to obtain high poling efficiency and piezoelectric properties without muffling. Further, $Na_2O$ volatilization occurred when NKN-based compositions were sintered at temperatures higher than 1000 °C, which presented difficulty in poling. Low temperature sintering was also required for 0.95NKN–0.05BT-based ceramics to achieve repeatable performance. Additionally, low temperature sintering is essential for the development of multilayer components. As shown in Table 7, good additives were developed and the effect of $MnO_2$ and CuO addition on the microstructure and piezoelectric/dielectric properties was quantified.

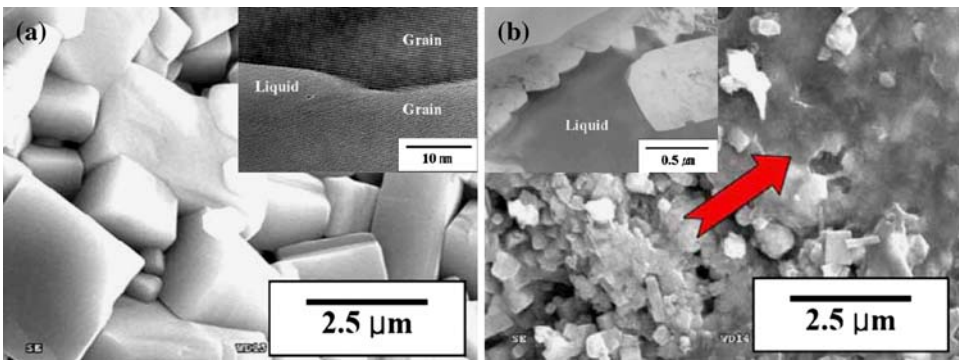


**Fig. 9** SEM and TEM images of $0.95(Na_{0.5}K_{0.5})NbO_3$–$0.05BaTiO_3$ ceramics sintered at various temperatures for 2 h. (**a**) 1060 °C and (**b**) 1125 °C

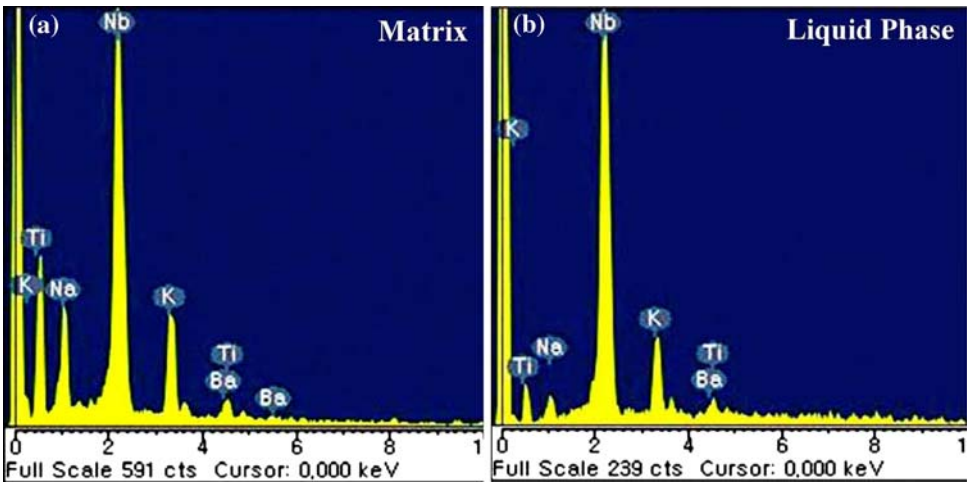


**Fig. 10** EDS spectra taken from the (**a**) matrix and (**b**) liquid phases of $0.95(Na_{0.5}K_{0.5})NbO_3$–$0.05BaTiO_3$ ceramics sintered at 1125 °C

**Table 4** Chemical compositions of the matrix and the liquid phases of $0.95(Na_{0.5}K_{0.5})NbO_3$–$0.05BaTiO_3$ ceramics sintered at 1125 °C [41]

| Element | Matrix | | Liquid phase | |
|---|---|---|---|---|
| | Weight% | Atomic% | Weight% | Atomic% |
| Na | 8.41 | 23.01 | 2.21 | 7.12 |
| K | 16.14 | 25.96 | 13.73 | 25.96 |
| Nb | 66.85 | 45.24 | 77.62 | 61.78 |
| Ba | 6.42 | 2.85 | 4.77 | 2.57 |
| Ti | 2.17 | 2.94 | 1.67 | 2.57 |

**Table 5** Chemical composition of the liquid phase as calculated by Eq. 1 [41]

| Element | Atomic% |
|---|---|
| Na | 7.12 |
| K | 29.39 |
| Nb | 58.39 |
| Ba | 2.55 |
| Ti | 2.55 |

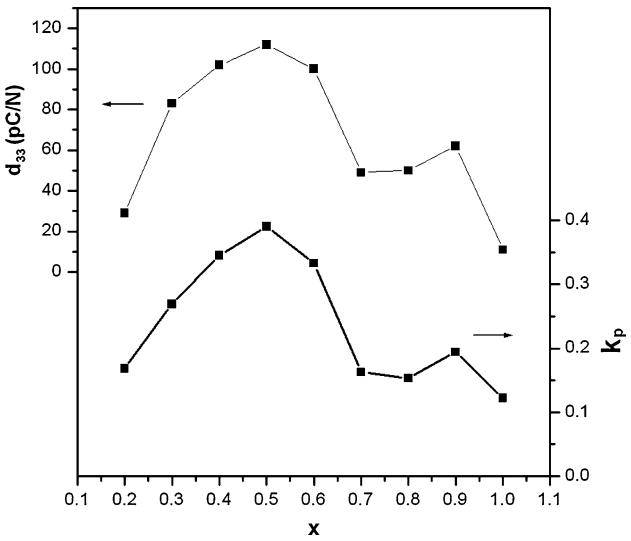


**Fig. 11** Piezoelectric properties of $(Na_{1-x}K_x)NbO_3$ ceramics

Figure 17 shows the X-ray diffraction patterns and SEM image of 0.95NKN–0.05BT and 0.95NKN–0.05BT + 0.5 mol% $MnO_2$ ceramics sintered at 1050 °C for 2 h. All the peaks were indexed as perovskite and no secondary phase was detected. $MnO_2$-modified specimens showed higher density of 95.5% compared to ~90% of 0.95NKN–0.05BT ceramics sintered at 1060 °C. Thus, the improvement of piezoelectric properties might be due to increased density. Figure 18 shows the variation of dielectric constant as a function of temperature. The $T_c$ of 0.95NKN–0.05BT + 0.5 mol% $MnO_2$ ceramics was around 294 °C.

For CuO-added 0.95NKN–0.05BT specimen, no significant variation was found in X-ray diffraction patterns. However, liquid phase was found at the grain boundary, as

**Table 6** Piezoelectric and dielectric properties of $(Na_{0.5}K_{0.5})NbO_3$ + additives

| Additives (in NKN) | $d_{33}$ (pC/N) | $k_p$ | $\varepsilon_3^T/\varepsilon_0$ | $Q_m$ | $T_c$ (°C) | Sin. $T$. (°C) |
|---|---|---|---|---|---|---|
| None [46] | 115 | 0.39 | 330 | 107 | 420 | 1,090 |
| 1.0 mol% ZnO [46] | 123 | 0.40 | 500 | 145 | 400 | 1,050 |
| 0.9 mol% $MnO_2$ | 119 | 0.39 | 330 | 330 | – | 1,050 |
| 0.9 mol% $WO_3$ | 119 | 0.30 | 520 | 72 | – | 1,090 |
| 1.5 mol% CuO [52] | 100 | 0.36 | 220 | 1,200 | 400 | 950 |
| 1.5 mol% CuO + 3.0 mol% ZnO | 94 | 0.33 | 270 | 1,130 | – | 925 |

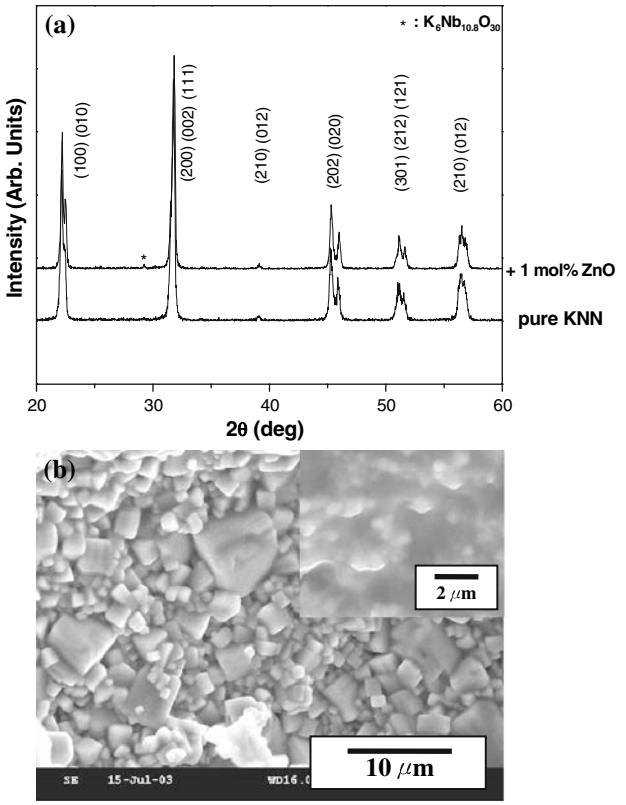


**Fig. 12** (**a**) X-ray diffraction pattern and (**b**) SEM image of $(Na_{0.5}K_{0.5})NbO_3$ + 1.0 mol% ZnO ceramics

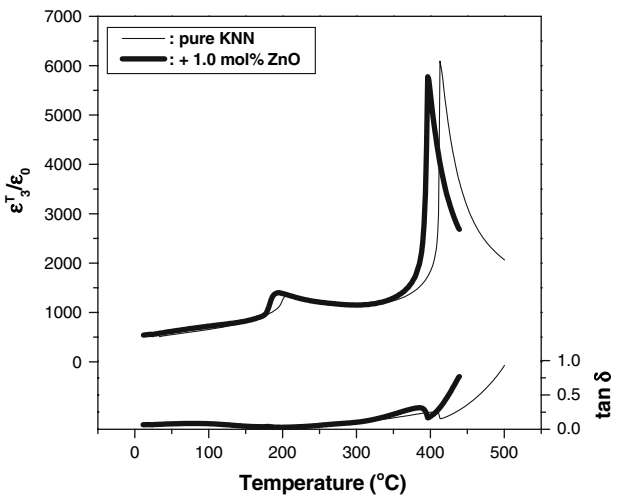


**Fig. 13** Variation of dielectric constant and loss factor as a function of temperature for $(Na_{0.5}K_{0.5})NbO_3 + x$ mol% ZnO ceramics (at 1 kHz)

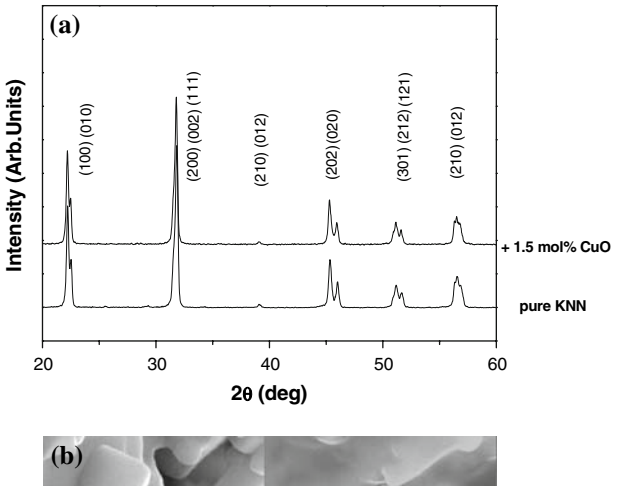


**Fig. 14** (**a**) X-ray diffraction pattern and (**b**) SEM image of $(Na_{0.5}K_{0.5})NbO_3$ + 1.5 mol% CuO ceramics

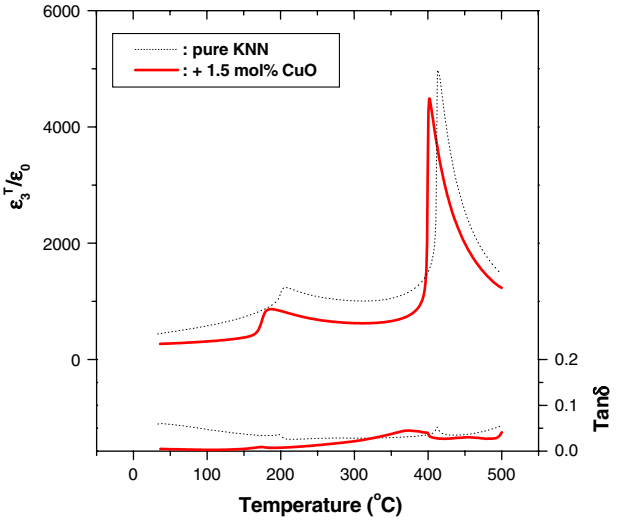


**Fig. 15** Variation of dielectric constant and loss factor as a function of temperature for $(Na_{0.5}K_{0.5})NbO_3 + x$ mol% CuO ceramics (at 100 kHz)

shown in Fig. 19. Thus, the low sintering temperature and large size grains can be explained by the formation of liquid phase in CuO-added 0.95NKN–0.05BT ceramics. The Curie temperature of CuO-added 0.95NKN–0.05BT ceramics was approximately 286 °C, as shown in Fig. 20. In order to further improve the microstructure and piezoelectric properties of CuO-added 0.95NKN–0.05BT ceramics, $MnO_2$ was selected as the secondary dopant. Figure 21 shows the X-ray diffraction pattern and microstructure of 0.95NKN−0.05BT + 2.0 mol% CuO + 0.5 mol% $MnO_2$ ceramics sintered at 950 °C for 10 h. All the peaks were indexed as perovskite and no evidence of secondary phase was found. Moreover, a

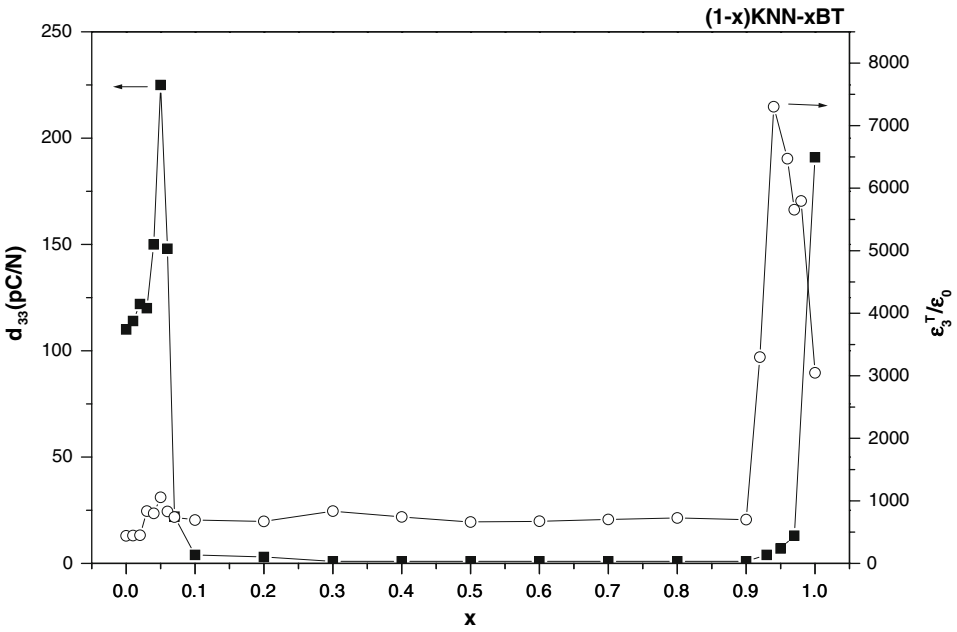


**Fig. 16** Piezoelectric and dielectric constant of $(1 - x)(Na_{0.5}K_{0.5})NbO_3$–$xBaTiO_3$ ceramics

**Table 7** Piezoelectric and dielectric properties of $0.95(Na_{0.5}K_{0.5})NbO_3$–$0.05BaTiO_3$ + additives

| Additives (in 0.95NKN–0.05BT) | $d_{33}$ (pC/N) | $k_p$ | $\varepsilon_3^T/\varepsilon_0$ | $Q_m$ | $T_c$ (°C) | Sin. $T$. (°C) |
|---|---|---|---|---|---|---|
| None [40, 41] | 225 | 0.36 | 1,058 | 74 | 320 | 1,060 |
| 0.5 mol% $MnO_2$ [53] | 237 | 0.42 | 1,252 | 92 | 294 | 1,050 |
| 1.0 mol% ZnO | 220 | 0.36 | 1,138 | 71 | – | 1,040 |
| 2.0 mol% CuO [47, 54] | 220 | 0.34 | 1,282 | 186 | 286 | 950 |
| 2.0 mol% CuO + 0.5 mol% $MnO_2$ [54] | 248 | 0.41 | 1,258 | 305 | 277 | 950 |

narrow grain size distribution was found compared to that of CuO-added 0.95NKN–0.05BT specimens. The liquid phase could not be detected at grain boundaries when $MnO_2$ was added to 0.95NKN–0.05BT + 2.0 mol% CuO ceramics. Piezoelectric properties were improved in $MnO_2$–added 0.95NKN–0.05BT + 2.0 mol% CuO ceramics, as shown in Table 7. This enhancement might be due to the formation of homogeneous microstructure compared with CuO-added 0.95NKN–0.05BT ceramics. A high density of 95% was obtained at the low sintering temperature of 950 °C for CuO- and $MnO_2$- modified 0.95NKN–0.05BT ceramics. In addition, the composition modified with 2.0 mol% CuO and 0.5 mol% $MnO_2$ was found to exhibit high magnitude of dielectric and piezoelectric properties as shown in Table 7. The Curie temperature for this composition was approximately 277 °C, as shown in Figs. 22 and 23.

## Dielectric properties: NKN–BT ceramics for capacitor applications [48]

The rapid development of the mobile electronic equipments requires miniaturization of high performance multilayer ceramic capacitor (MLCC). This requirement can be achieved by developing thin dielectric layer with high capacitance and fine grain size. According to electronic industries association (EIA), for 0402 (1.0 mm × 1.0 mm × 0.5 mm) with capacitance of 10 μF, the thickness of one dielectric layer should be less than 1 μm with a dielectric constant more than 7000. The results on the $(1 - x)$NKN–$x$BT ceramics (BT-rich) fit this criterion as they exhibit small grain size (<0.5 μm) and large dielectric constant of higher than 7000 (Figs. 3b, 7, 16 and, 23). The composition 0.06NKN–0.94BT lies on the boundary of the tetragonal and cubic phases as seen in Fig. 1c. This composition showed a large dielectric constant of 7500 at room temperature and a loss factor of less than 1% in the temperature range between −20 and 130 °C, as shown in Figs. 3b and 23. The average grain size was of the order 0.4 μm.

## Conclusion

The phase transition, microstructure, and piezoelectric/dielectric properties of $(1 - x)$NKN–$x$BT ceramics

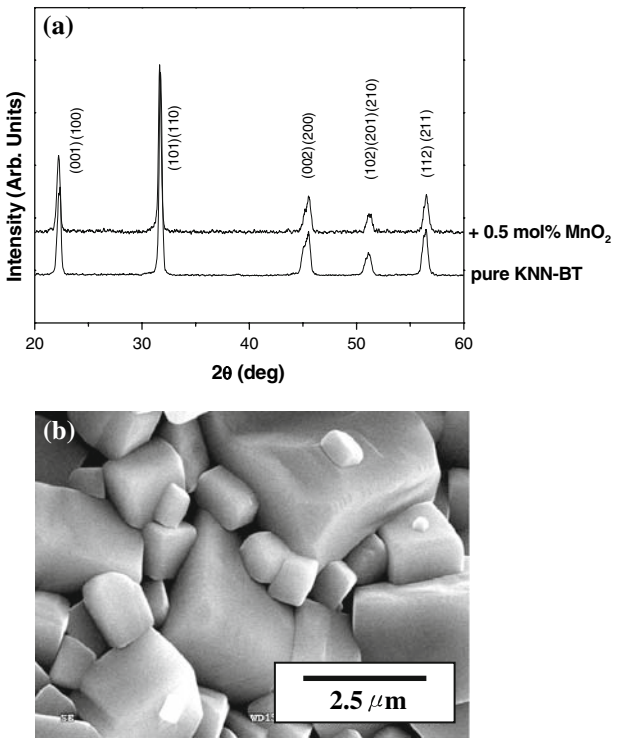


**Fig. 17** (**a**) X-ray diffraction pattern and (**b**) SEM image of $0.95(Na_{0.5}K_{0.5})NbO_3$–$0.05BaTiO_3$ + 0.5 mol% $MnO_2$ ceramics

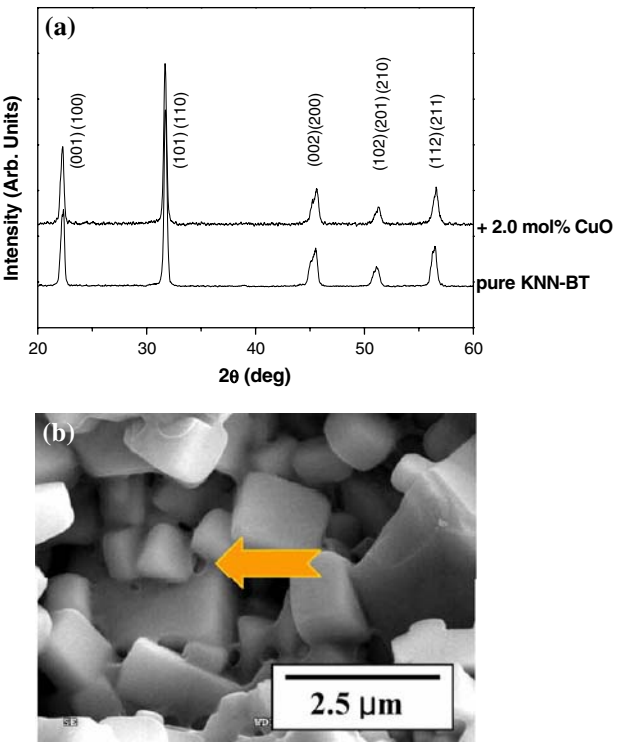


**Fig. 19** (**a**) X-ray diffraction pattern and (**b**) SEM image of $0.95(Na_{0.5}K_{0.5})NbO_3$–$0.05BaTiO_3$ + 2.0 mol% CuO ceramics

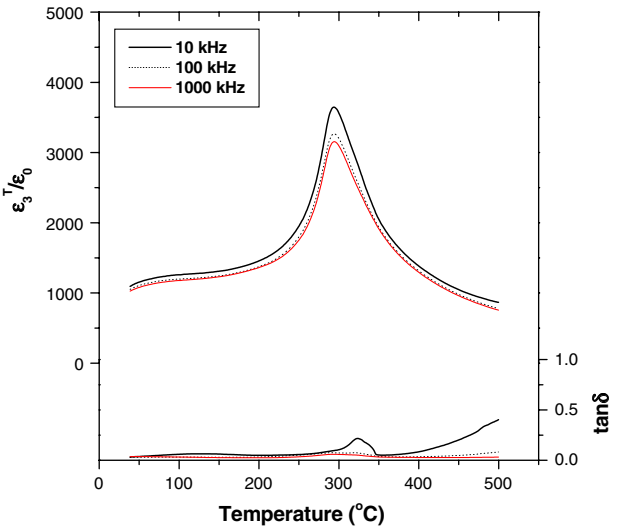


**Fig. 18** Variation of dielectric constant and loss factor as a function of temperature for $0.95(Na_{0.5}K_{0.5})NbO_3$–$0.05BaTiO_3$ + 0.5 mol% $MnO_2$ ceramics (at 100 kHz)

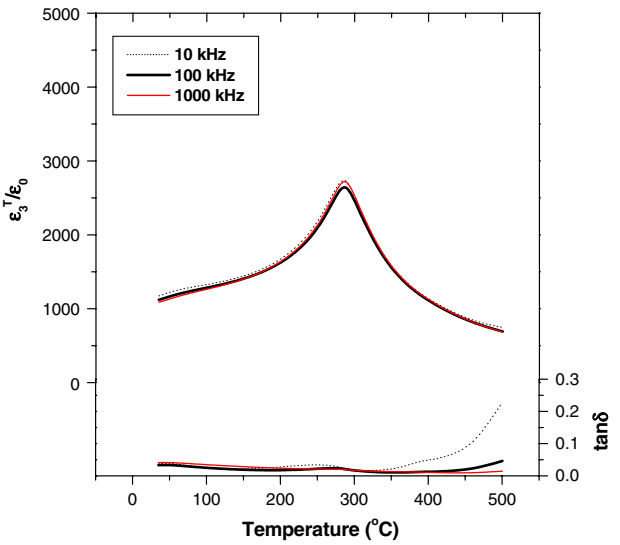


**Fig. 20** Variation of dielectric constant and loss factor as a function of temperature for $0.95(Na_{0.5}K_{0.5})NbO_3$–$0.05BaTiO_3$ + 2.0 mol% CuO ceramics

($0.0 \leq x \leq 1.0$) were reviewed. The phase transitions in $(1 - x)$NKN–$x$BT ceramics were analyzed using X-ray diffraction and the dielectric and ferroelectric properties, and are summarized over the whole composition range in Fig. 24. Three phase transition regions were found in $(1 - x)$ NKN–$x$BT ceramics. In the NKN-rich region, there is a boundary between the orthorhombic and tetragonal phases. The composition corresponding to this boundary, 0.95NKN–0.05BT, exhibited excellent dielectric and piezoelectric properties. However, 0.95NKN–0.05BT ceramics show low poling efficiency due to low resistivity. Modification with additives improved poling efficiency and

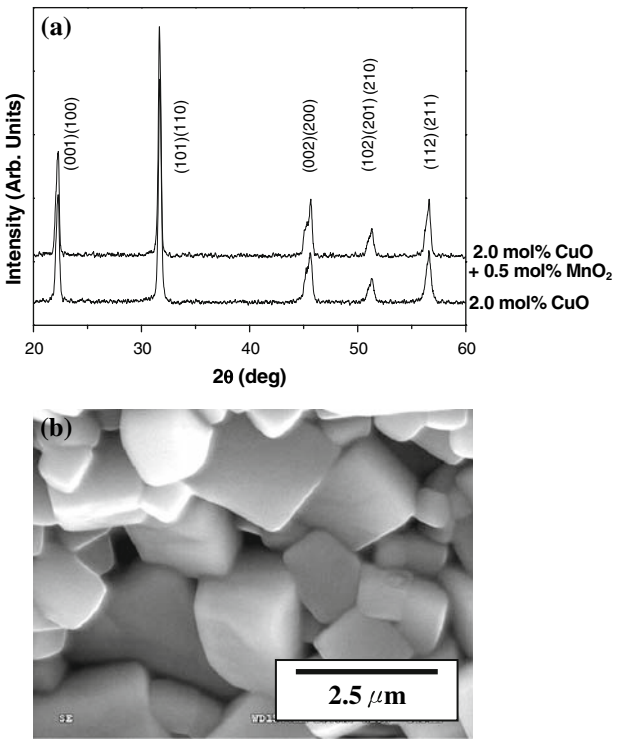


**Fig. 21** (**a**) X-ray diffraction pattern and (**b**) SEM image of $0.95(Na_{0.5}K_{0.5})NbO_3$–$0.05BaTiO_3$ + 2.0 mol% CuO + 0.5 mol% $MnO_2$ ceramics

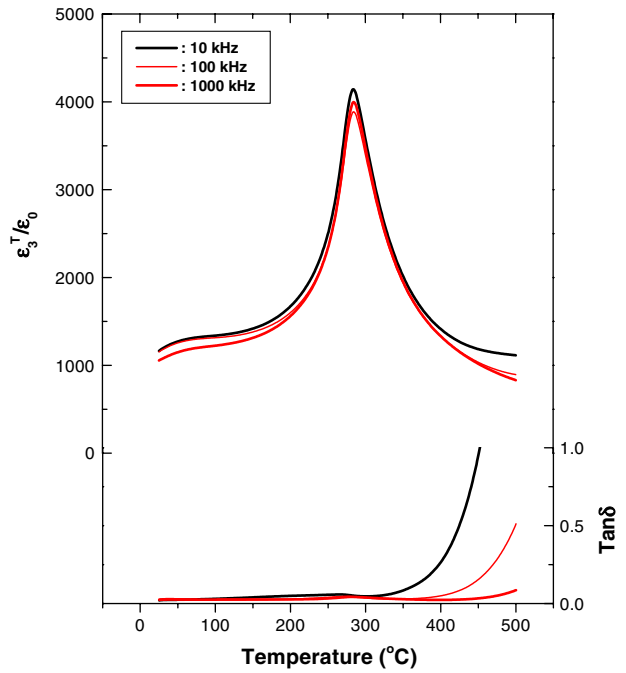


**Fig. 22** Variation of dielectric constant and loss factor as a function of temperature for $0.95(Na_{0.5}K_{0.5})NbO_3$–$0.05BaTiO_3$ + 2.0 mol% CuO + 0.5 mol% $MnO_2$ ceramics

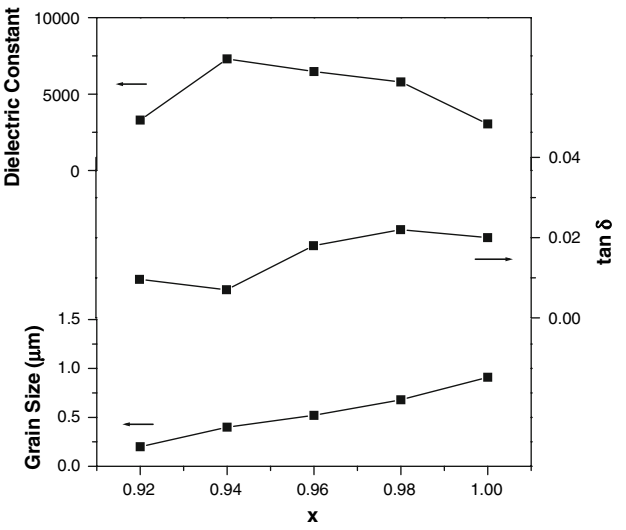


**Fig. 23** Dielectric constant, tan $\delta$, and grain size of $(1 - x)(Na_{0.5}K_{0.5})NbO_3$–$xBaTiO_3$ ceramics: $0.92 \leq x \leq 1.00$, dielectric constant and tan $\delta$ at 30 °C

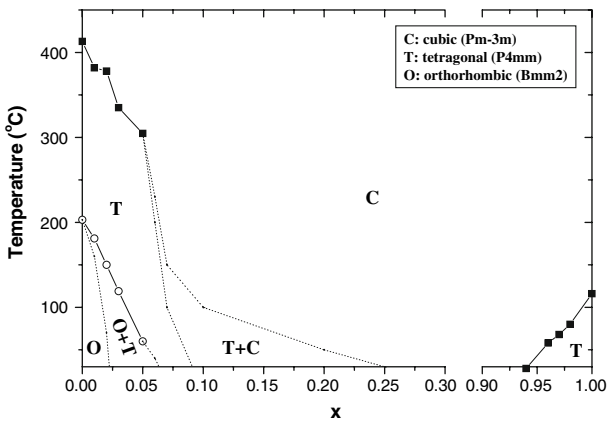


**Fig. 24** Schematic diagram of phase transition for $(1 - x)(Na_{0.5}K_{0.5})NbO_3$–$xBaTiO_3$ ceramics

resulted in excellent piezoelectric properties. In the BT-rich region, there is a boundary between the tetragonal and cubic phases. The composition corresponding to this boundary, 0.06NKN–0.94BT, exhibited a microstructure with small grain size and excellent dielectric properties. In the central regime ($0.25 < x < 0.93$), the ceramics exist in a cubic phase. The results on this system clearly demonstrate that $(1 - x)$NKN–$x$BT ceramics are promising candidates for lead-free dielectric and piezoelectric devices.

**Acknowledgements** The authors gratefully acknowledge the financial support from the office of Basic Energy Science, Department of Energy.

## References


1. Haertling GH (1999) J Am Ceram Soc 82(4):797
2. Shrout TR, Zhang SJ (2007) J Electroceram 19:111
3. Saito Y, Takao H, Tani T, Nonoyama T, Takatori K, Homma T et al (2004) Nature 432:84. doi:10.1038/nature03028
4. Hollenstein E, Davis M, Damjanovic D, Setter N (2005) Appl Phys Lett 87:182905. doi:10.1063/1.2123387
5. Saito Y, Takao H (2006) Ferroelectrics 338:17. doi:10.1080/00150190600732512
6. Wang R, Xie R, Hanada K, Matsusaki K, Bando H, Itoh M (2005) Phys Status Solidi A Appl Res 202:R57. doi:10.1002/pssa.200510014
7. Hollenstein E, Damjanovic D, Setter N (2007) J Eur Ceram Soc 27:4093. doi:10.1016/j.jeurceramsoc.2007.02.100
8. Zhao P, Zhang BP, Li JF (2007) Appl Phys Lett 91:172901. doi:10.1063/1.2794405
9. Guo Y, Kakimoto K, Ohsato H (2004) Appl Phys Lett 85:4121. doi:10.1063/1.1813636
10. Zang GZ, Wang JF, Chen HC, Su WB, Wang CM, Qi P et al (2006) Appl Phys Lett 88:212908. doi:10.1063/1.2206554
11. Lang SB, Zhu W, Cross LE (2006) Ferroelectrics 336:15. doi:10.1080/00150190600695115
12. Takao H, Saito Y, Aoki Y, Horibuchi K (2006) J Am Ceram Soc 89:1951. doi:10.1111/j.1551-2916.2006.01042.x
13. Lin D, Kwok KW, Tian H, Wong H, Chan L-W (2007) J Am Ceram Soc 90(5):1458. doi:10.1111/j.1551-2916.2007.01627.x
14. Zhang S, Xia R, Shrout TR, Zang G, Wang J (2006) J Appl Phys 100:104108. doi:10.1063/1.2382348
15. Matsubara M, Kikuta K, Hirano S (2005) J Appl Phys 97:114105. doi:10.1063/1.1926396
16. Matsubara M, Yamaguchi T, Sakamoto W, Kikuta K, Yogo T, Hirano S (2005) J Am Ceram Soc 88:1190. doi:10.1111/j.1551-2916.2005.00229.x
17. Yoo J, Hong J, Lee H, Jeong Y, Lee B, Song H et al (2006) Sens Actuators A Phys 126:41. doi:10.1016/j.sna.2005.09.005
18. Choy SH, Wang XX, Chan HLW, Choy CL (2006) Appl Phys A 82:715. doi:10.1007/s00339-005-3421-z
19. Yuan Y, Zhang S, Zhou X, Liu J (2006) Jpn J Appl Phys 45:831. doi:10.1143/JJAP.45.831
20. Lin D, Xiao D, Zhu J, Yu P (2006) Appl Phys Lett 88:062901. doi:10.1063/1.2171799
21. Wang XX, Tang XG, Chan HLW (2004) Appl Phys Lett 85:91. doi:10.1063/1.1767592
22. Hiruma Y, Aoyagi R, Nagata H, Takenaka T (2004) Jpn J Appl Phys 43:7556. doi:10.1143/JJAP.43.7556
23. Takenaka T, Nagata H (1999) Key Eng Mater 157–158:57
24. Takenaka T, Nagata H (2005) J Eur Ceram Soc 25:2693. doi:10.1016/j.jeurceramsoc.2005.03.125
25. Choy SH, Wang XX, Chan HLW, Choy CL (2006) Ferroelectrics 336:69. doi:10.1080/00150190600695784
26. Song JS, Jeong SJ, Kim IS, Lee DS, Park EC (2006) Ferroelectrics 338:3. doi:10.1080/00150190600732470
27. Zeng JT, Kwok KW, Chan HLW (2006) J Am Ceram Soc 89:2828
28. Wang X, Chan HLW, Choy CL (2003) Solid State Commun 125:395. doi:10.1016/S0038-1098(02)00816-5
29. Zhao S, Li G, Ding A, Wang T, Yin Q (2006) J Phys D Appl Phys 39:2277. doi:10.1088/0022-3727/39/10/042
30. Takenaka T, Maruyama K, Sakata K (1991) Jpn J Appl Phys 30:2236. doi:10.1143/JJAP.30.2236
31. Nagata H, Yoshida M, Makiuchi Y, Takenaka T (2003) Jpn J Appl Phys 42:7401. doi:10.1143/JJAP.42.7401
32. Hiruma Y, Makiuchi Y, Aoyagi R, Nagata H, Takenaka T (2006) Ceram Trans 174:139
33. Wu L, Xiao D, Lin D, Zhu J, Yu P (2005) Jpn J Appl Phys 44:8515. doi:10.1143/JJAP.44.8515
34. Lin D, Xia D, Zhu J, Yu P (2005) Phys Status Solidi A Appl Res 202:R89. doi:10.1002/pssa.200510034
35. Wang R, Tachibana N, Miura N, Hanada K, Matsusaki K, Bando H et al (2006) Ferroelectrics 331:135. doi:10.1080/00150190600737693
36. Maeder MD, Damjanovic D, Setter N (2004) J Electroceram 13:385
37. Chen W, Li Y, Xu Q, Zhou J (2005) J Electroceram 15:229. doi:10.1007/s10832-005-3301-0
38. Berlincourt D (1971) In: Mattiat OE (ed) Ultrasonic transducer materials: piezoelectric crystals and ceramics. Plenum, London, ch. 2
39. Ming BQ, Wang JF, Qi P, Zang GZ (2007) J Appl Phys 101:054103. doi:10.1063/1.2436923
40. Park HY, Ahn CW, Song HC, Lee JH, Nahm S, Uchino K et al (2006) Appl Phys Lett 89:062906. doi:10.1063/1.2335816
41. Ahn CW, Park HY, Nahm S, Uchino K, Lee HG, Lee HJ (2007) Sens Actuators A Phys 136:255. doi:10.1016/j.sna.2006.10.036
42. Cho KH, Park HY, Ahn CW, Nahm S, Lee HG, Lee HJ (2007) J Am Ceram Soc 90(6):1946. doi:10.1111/j.1551-2916.2007.01715.x
43. Park HY, Cho KH, Paik DS, Nahm S, Lee HG, Kim DH (2007) J Appl Phys 102:124101. doi:10.1063/1.2822334
44. Ahn CW, Song HC, Nahm S, Park SH, Uchino K, Priya S et al (2005) Jpn J Appl Phys 44(44):L1361. doi:10.1143/JJAP.44.L1361
45. Shimojo Y, Wang R, Sekiya T, Matsuzaki K (2005) J Korean Phys Soc 46(1):48
46. Park SH, Ahn CW, Nahm S, Song JS (2004) Jpn J Appl Phys 43:L1072
47. Park HY, Ahn CW, Cho KH, Nahm S, Lee HG, Kang HW et al (2007) J Am Ceram Soc 90(12):4066
48. Choi CH, Ahn CW, Nahm S, Hong JO, Lee JS (2007) Appl Phys Lett 90:132905
49. Raseand DE, Roy R (1953) The Pennsylvania State University, College of Mineral Industries; Eighth Quarterly Progress Report, April 1 to June 30, Appendix II, 16
50. Irleand E, Blachnik R (1991) Thermochim Acta 185(2):355. doi:10.1016/0040-6031(91)80056-O
51. Wu L, Wu TS, Wei CC, Liu HC (1983) J Phys C Solid State Phys 16:2823. doi:10.1088/0022-3719/16/14/022
52. Ahn CW, Karmarkar M, Viehland D, Kang DH, Bae KS, Priya S, Ferroelectrics (accepted)
53. Ahn CW, Nahm S, Yoo MJ, Lee HG, Priya S (2008) J Mater Sci 43:6016
54. Ahn CW, Nahm S, Karmarkar M, Viehland D, Kang DH, Bae KS et al (2008) Mater Lett 62:3594